Q tomography towards true amplitude image and improve sub-karst image

Yang He and Jun Cai, TGS

Summary

A frequency domain tomographic inversion was developed to estimate frequency dependent energy attenuation by using prestack depth migration common image gathers (CIGs). The frequency dependent attenuation is estimated from the centroid frequency difference for reflections in CIGs. Migration stretch and ghost effects are taken into account to get correct measurements of frequency. This method makes correction for these factors to obtain correct frequency difference, utilizes the actual ray paths and avoids using amplitude information. It is relatively insensitive to some of amplitude loss factors, such as geometric spreading, reflection and transmission loss, source and receiver radiation patterns. Q tomography was used to derive the Q model for karst media. The compensation of amplitude loss improves the sub-karst amplitude fidelity.

Introduction

The propagation of seismic wave through the earth is affected by attenuation due to inelastic nature. Assuming attenuation is linearly dependent on frequency and Q is independent on frequency, amplitude spectra change after attenuation. The high frequencies of the seismic signal are attenuated more than the low frequencies. The changes in seismic amplitude spectra serve as observed data for attenuation estimation.

Attenuation of the received signals is determined by its propagation path through the Q model. Taking actual ray path information into account, Q model is estimated by tomographic inversion. Q tomography algorithms are classified into two main categories based on how data info is used. One category utilizes amplitude-spectra-ratio method for estimating Q. The natural log spectra ratio between reflections with and without attenuation gives estimation of Q model (Dasgupta and Clark 1998). But many factors affect amplitudes, including scattering, geometric spreading, source and receiver directivity, radiation patterns and transmission /reflection effects. These factors are assumed to be frequency independent, which are difficult to exclude. The other category measures the relative shift of the centroid or dominant frequency of the signal spectrum. It might obtain reliable attenuation estimates from the relative measurements. Quan and Harris (1997) developed a method for estimating seismic attenuation based on frequency shift data. They derived the relationship between Q model and centroid frequency shift for Gaussian, boxcar and triangular spectra. Zhang and Ulrych (2002) derived an analytical relationship between Q-factor and seismic data peak frequency variation for a Ricker wavelet. Hu et al. (2011) designed a source-amplitude spectrum fitting function to handle asymmetric source amplitude spectra. The shape and the bandwidth of the function are determined by two parameters separately, which makes it convenient to fit various asymmetric source amplitude spectra. The measurement based on frequency shifts could be more reliable when absolute amplitude is not used.

These frequency Q estimation methods are done in data domain, obtaining interval attenuation directly from prestack gathers by measuring frequency of seismic signals. Picking prestack events on complex data is considered unfeasible, because of low signal-to-noise level or complex arrivals related to heterogeneous velocity models. Differing from previous approaches, we operate on depth migrated CIG gathers in imaging domain. The key of our approach is to obtain centroid frequency difference from 3D prestack depth migrated CIG gathers. After obtaining the frequency difference, they can be used as observed data to reconstruct the attenuation distribution tomographically.

Method

To obtain correct centroid frequency from depth migrated gathers, we need to make corrections for migration stretch first. Migration stretch is created when mapping an input time source wavelet to its equivalent vertical depth. It causes loss of frequency bandwidth and wavelet distortion. There are a number of factors affecting the stretch of events in depth, such as reflection angle, structure dip and local velocity.

With some geometry analysis, migration stretch is related to incident angle, which suggests that working in common angle domain is advantageous. So we mapped the common offset gathers into common angle gathers and extracted frequency from angle-dependent reflections.

Figure 1a displays a CIG gather created by Kirchhoff prestack depth migration with a gradient velocity. The offset range is about twice that of the depth. Note that stretch at far offsets is more evident than near offsets at shallow depth where incident are large. Also the stretch varies with depth at a given offset. Besides, the reflection in the deep is wider because the velocity is higher. The migration stretch is described as the following equation,

$$\frac{dz'}{dz} = \frac{1}{\cos(\theta)\cdot\cos(\alpha)}\cdot\frac{v}{v_r}$$

DOI http://dx.doi.org/10.1190/segam2012-1220.1

where θ is incident angle between imaging ray path and structure reflection plane, α is dipping angle of structure plane, and v is local velocity at reflection point, v_r is reference velocity at reference location. dz is the sample interval at reference location. The ratio of dz' and dz represents migration stretch. dz' is used to resample the gathers to un-stretch the reflection events in depth. Figure 1b displays the un-stretched gathers. Note that after un-stretching, all reflections from different offsets and depth have the same thickness in depth. Structure dip is picked from stacking images and used for correction for dipping reflections.

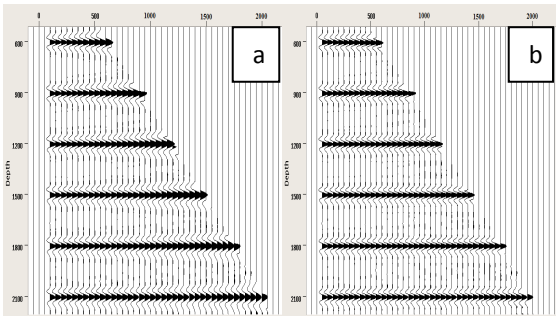

Figure 1: a) Gather from Kirchhoff Depth Migration. b) Gather after un-stretching.

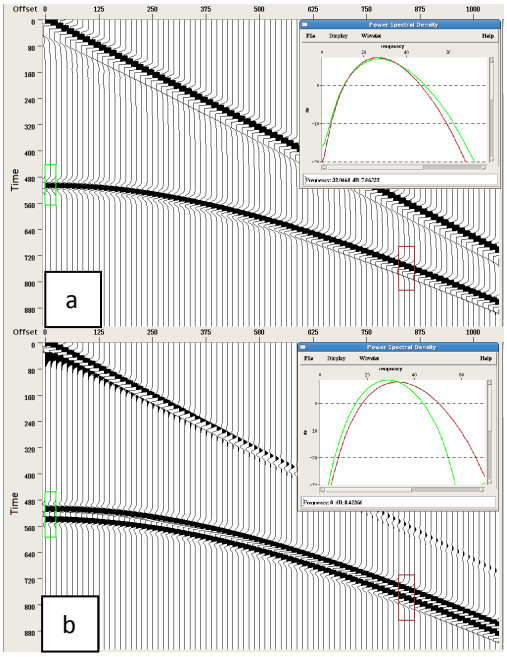

Figure 2: a) A shot gather for a horizontal reflection with absorbing boundary. b) with free surface boundary.

Besides migration stretch, source and receiver have frequency-dependent directivity due to surface ghosts (Hustedt and Clark, 1999). Figure 2 displays a comparison of shot gathers for two boundary conditions. The modeled spectra are clearly affected by directivity. The far offset appears to be of higher frequency than the near offset. The surface of the ocean acts as an acoustic mirror, causing ghost effects in recorded seismic data. The time delay between the primary wavefield and the ghost wavefield varies with take-off angle from source and incident angle at receiver, thus leads to frequency-dependent directivity. Figure 3 displays a comparison of CIG gathers migrated for synthetic data with absorbing and free-surface boundary conditions. The dominant frequency shift in the gather with free-surface boundary condition is less evident than the one with absorbing boundary because ghost effects appear to suppress the stretch. The presence of ghost complicates the Q estimation. To make correction for the ghost effect, frequency change with directions is accounted to obtain the correct centroid frequency.

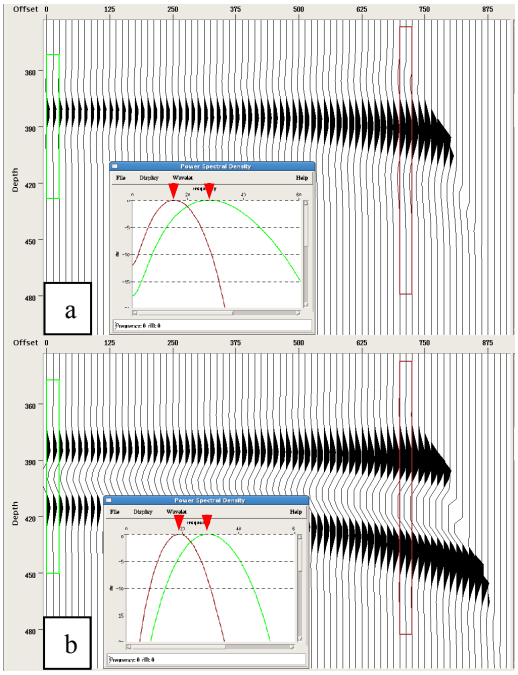

Figure 3: a) Common offset gather with absorbing boundary. b) with free surface boundary. Note the spectra comparison for near and far offsets.

First, a clean source wavelet needs to be estimated. Direct arrival is characterized by a source wavelet plus its ghost reflection from the air-water interface. The time delay between them is small when the depth of source and receiver is small. The source wavelet and the ghost are of opposite sign in amplitude and their amplitudes are almost

DOI http://dx.doi.org/10.1190/segam2012-1220.1

of the same magnitude due to almost perfect mirror reflection from air-water interface. Thus the direct arrival is a derivative of the clean source wavelet (Niu, personal communication). By integration of direct arrival, the source wavelet can be estimated. For each reflection picked in CIGs, take-off angle from source and incident angle at receiver were computed and the surface ghost spectral responses due to source and receiver were evaluated and corrected from the measured frequency.

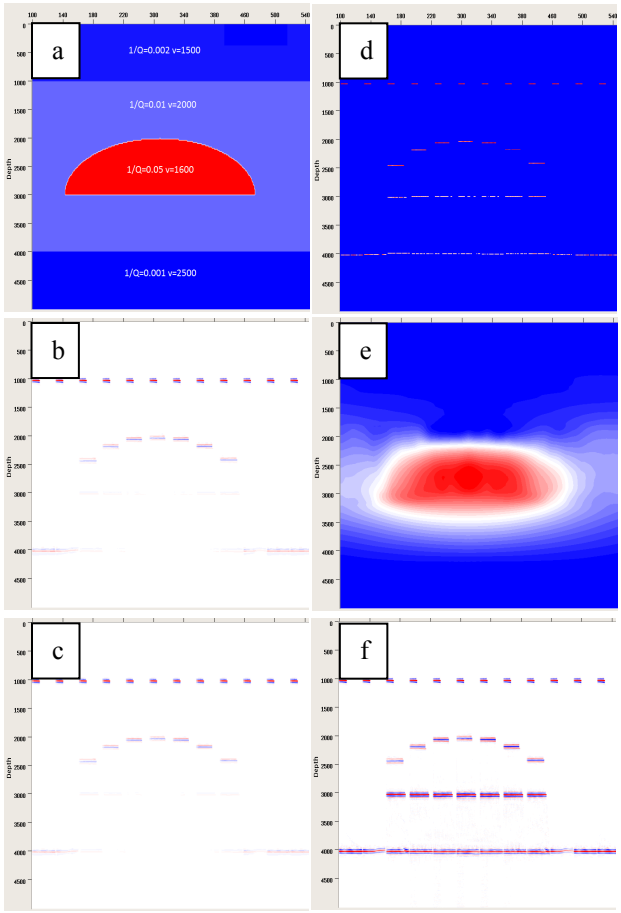

Figure 4: a) Model with 1/Q and velocity labeled. b) Gather from conventional Kirchhoff Prestack Depth Migration. c) Gather after un-stretching. d) Picked frequency displayed on gather. e) Reconstructed 1/Q model displayed with same scale as a. f) Gather after Q migration.

Residual frequency shift after un-stretching and ghost-correction of picked reflections along the moveout curves serves as the input data to estimate the interval Q. The downshift in centroid frequency is proportional to a path integral through the attenuation distribution. Seismic attenuation effect can be quantitatively estimated by Q tomography.

Examples

First we verify the validity of our frequency approach with a synthetic test. Figure 4a shows a two dimensional earth model of three horizontal layers and a gas pocket in which Q properties are labeled. For conventional migration, Figure 4b shows both amplitude and frequency loss for the reflection beneath the attenuation zone. Figure 4c shows the un-stretched gathers after migration stretch is removed. For detail, Figure 5 is a zoom-in display for 3 locations of Figure 4c. The reflection in the middle (Figure 5b) beneath

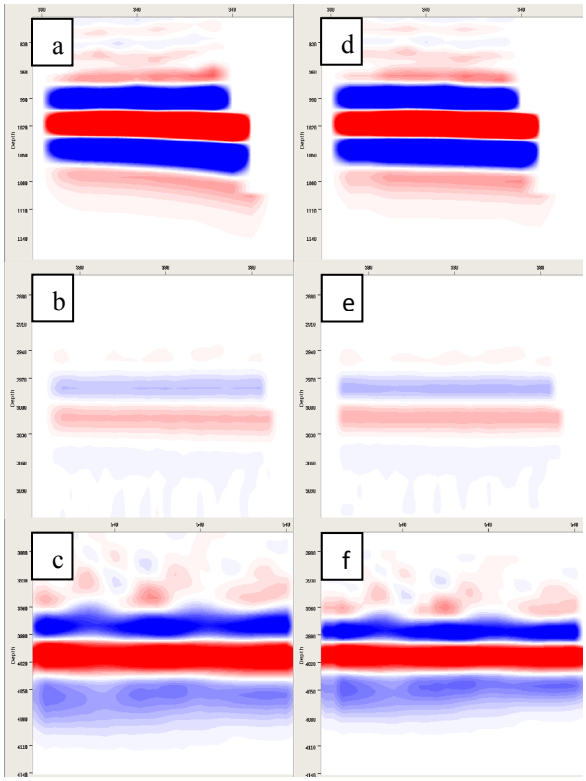

Figure 5: Zoom-in display of the gather before (a,b,c) and after un-stretching (d,e,f) for figure 4b and 4c.

the attenuation zone is broadened in comparison to the reflection on the right (Figure 5c). The reflections after attenuation (Figure 5b, c) have phase change in comparison to non-attenuated reflection (Figure 5a). Figure 4d shows the centroid frequency picked on the un-stretched gathers. Note that the frequency pattern through the model gives indication of the high attenuation zone. On the edge of the gas pocket, strong migration swing is observed. The cross-correlation value of the gather and the stack is used with a

DOI http://dx.doi.org/10.1190/segam2012-1220.1

threshold to control the quality of the picking. Figure 4e shows the estimated Q model, in which Q anomalies are well recovered though there is some smoothing leakage along boundary. Figure 4f shows the gather after Q migration. The amplitude and frequency content of the reflections beneath the attenuation zone is well compensated. Also note that the phase is correct.

Next step is to test it with field data. For Hernando survey in the eastern Gulf of Mexico, carbonate karst zones are often found over the Florida Escarpment shown in Figure 6. The karst zones have significantly slower velocities than the surrounding sediments. The size of these karsts is usually a few meters to a few hundred meters. Attenuation in karst zones can be high due to fractures and unconsolidated rock, causing the amplitude dimming beneath it.

Spectral measurements of the reflections are complicated by interference effects resulting from closely spaced events. To build Q model in karst zone, two isolated horizons are picked in the deep to avoid adjacent reflections. Frequency measurement is completed for the reflections along the horizons after migration stretch and ghost effects are removed. Then the frequency shift is used for inversion of Q model. Figure 6d shows the reconstructed 1/Q anomalies. The estimated Q model then is used in Q migration to compensate the amplitude and frequency loss in imaging. Figure 6b shows the stacking image after Q migration.

Conclusions

We have developed a frequency domain tomographic inversion to estimate quality factor Q. The data used to estimate attenuation is extracted from the centroid frequency difference of reflections in prestack depth migrated CIGs. Migration stretch and ghost effects are corrected to obtain the centroid frequency difference between migration gathers from different depth, locations and offsets. This method utilizes the actual ray paths and avoids using amplitude information. The synthetic and real data examples validate this attenuation tomography and show its effect in amplitude and frequency compensation.

Acknowledgments

Authors would like to thank Sang Suh and Shuqian Dong for generating the synthetic data. Thank Hao Xun, Zhiqiang Guo, Xiansong Zeng and Bin Wang for helpful advice during this project, and Chuck Mason for proof reading. We thank the management of TGS for permission to publish this paper. The Hernando survey is a cooperative effort between TGS and PGS.

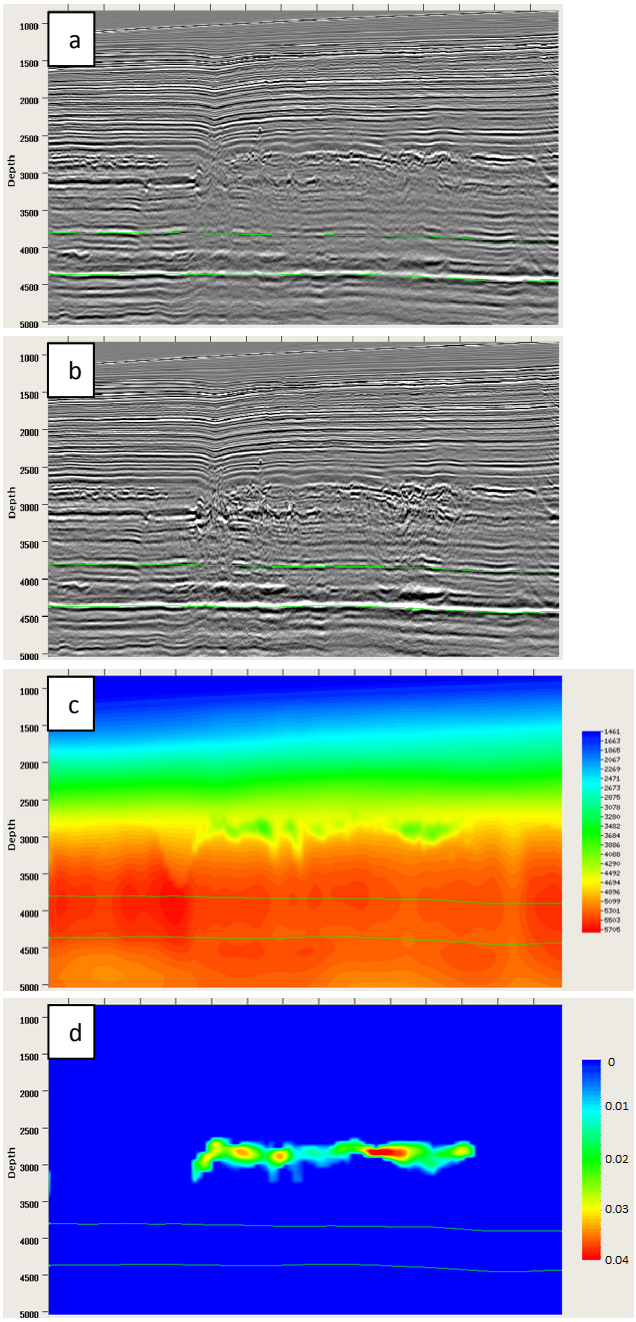

Figure 6: a) Stack image displayed with horizons overlaid. b) Stack image after Q migration. c) Velocity model of Karst zone with low velocity. d) 1/Q model estimated from Q tomography.

DOI http://dx.doi.org/10.1190/segam2012-1220.1

http://dx.doi.org/10.1190/segam2012-1220.1

EDITED REFERENCES

Note: This reference list is a copy-edited version of the reference list submitted by the author. Reference lists for the 2012 SEG Technical Program Expanded Abstracts have been copy edited so that references provided with the online metadata for each paper will achieve a high degree of linking to cited sources that appear on the Web.

REFERENCES

Dasgupta, R., and R. A. Clark, 1998, Estimation of Q from surface seismic reflection data: Geophysics, **63**, 2120-2128.

Hu, W., J. Liu, L. Bear, and C. Marcinkovich, 2011, A robust and accurate seismic attenuation tomography algorithm: SEG, Expanded Abstracts, **30**, 2727-2731.

Hustedt, B., and R. A. Clark, 1999, Source/receiver array directivity effects on marine seismic attenuation measurements: Geophysical Prospecting, **47**, 1105-1119.

Quan, Y., and J. M. Harris, 1997, Seismic attenuation tomography using the frequency shift method: Geophysics, **62**, 895-905.

Zhang, C. and T. J. Ulrych, 2002, Estimation of quality factors from CMP records: Geophysics, **67**, 1542-1547.

DOI http://dx.doi.org/10.1190/segam2012-1220.1